Least-Squares Phase Predistortion of a +30dBm Class-D Outphasing RF PA in 65nm CMOS

Ylva Jung, Jonas Fritzin, *Member, IEEE,* Martin Enqvist, *Member, IEEE,*
and Atila Alvandpour, *Senior Member, IEEE*

***Abstract*—This paper presents a model-based phase-only predistortion method suitable for outphasing radio frequency (RF) power amplifiers (PA). The predistortion method is based on a model of the amplifier with a constant gain factor and phase rotation for each outphasing signal, and a predistorter with phase rotation only. Exploring the structure of the outphasing PA, the model estimation problem can be reformulated from a nonconvex problem into a convex least-squares problem, and the predistorter can be calculated analytically. The method has been evaluated for 5 MHz Wideband Code-Division Multiple Access (WCDMA) and Long Term Evolution (LTE) uplink signals with Peak-to-Average Power Ratio (PAPR) of 3.5 dB and 6.2 dB, respectively, applied to one of the first fully integrated +30 dBm Class-D outphasing RF PA in 65nm CMOS. At 1.95 GHz for a 5.5 V (6.0 V) supply voltage, the measured output power of the PA was +29.7 dBm (+30.5 dBm) with a power-added efficiency (PAE) of 27 %. For the WCDMA signal with +26.0 dBm of channel power, the measured Adjacent Channel Leakage Ratio (ACLR) at 5 MHz and 10 MHz offsets were -46.3 dBc and -55.6 dBc with predistortion, compared to -35.5 dBc and -48.1 dBc without predistortion. For the LTE signal with +23.3 dBm of channel power, the measured ACLR at 5 MHz offset was -43.5 dBc with predistortion, compared to -34.1 dBc without predistortion.**

***Index Terms*—Outphasing, amplifier, linearization, predistortion, complementary metal-oxide-semiconductor (CMOS).**

I. Introduction

POWER amplifiers (PA) for modern wireless communications standards typically employ non-constant amplitude modulation schemes to use the limited frequency spectrum more efficiently and larger bandwidths to meet the demand for higher data rates. However, to meet the spectral and modulation requirements, highly linear PAs are required.

With the improved speed of CMOS transistors, highly efficient switched PAs, like Class-E and Class-D, have gained increased interest in polar modulation, shown for Enhanced Data rates for GSM Evolution (EDGE) [1], and outphasing [2], [3]. In the outphasing PA, an input signal, $s(t)$, containing both amplitude and phase modulation, is divided into two constant-envelope phase-modulated signals, $s_1(t)$ and $s_2(t)$, as in Fig. 1(a). Fig. 1(b) shows how the two signals are separately amplified by efficient switched amplifiers, A_1 and A_2, and connected to a power combiner whose output, $y(t)$, is an amplified replica of the input signal. The two constant amplitude outputs can be combined using an isolating combiner, like Wilkinson [4], or a non-isolating combiner, like Chireix [5] or transformers [6]. While an isolating combiner can have good linearity as the apparent load impedance for each amplifier is fixed [4], [7], the efficiency is reduced at back-off. With a non-isolating combiner, the apparent load impedance depends on the outphasing angle [8], degrading linearity if load-sensitive amplifiers are used [9], [10], but can help to reduce the power dissipation for small output amplitudes and improve the back-off efficiency [6]. As shown in [11]–[20], Class-D and Class-F amplifiers with non-isolating combiners can provide acceptable linearity.

Unless the amplifier stages, and signal paths, are identical, the amplifiers will experience gain and phase imbalances, creating nonlinearities and spectral distortion [5], [21], [22]. Earlier predistortion methods of RF PAs include model-based predistorters using model structures such as Volterra series [23]–[25], parallel Hammerstein structures [26], or look-up tables (LUT) [27], which also can be made adaptive [28], [29]. Compared to conventional linear PAs, the outphasing PA takes two constant envelope signals to create an amplitude and phase modulated output signal. Thus, there is no linearity between the individual outphasing signals and the output, and new predistortion methods are needed.

Phase-predistortion was evaluated for Chireix combiners in simulations and by using signal generators in measurements (no PA was used) in [5]. To compensate for the gain mismatch, earlier proposed predistorters changed the input signal amplitudes when linear amplifiers were used [30]–[32], or included adjustments of the voltage supplies in the output stage [8], [9]. In [16], an amplifier model and predistorter were proposed to compensate for amplitude and phase mismatches by changing only the phases of the two input outphasing signals, evaluated for uplink signals with PAPR of ~3.5 dB applied to a +10 dBm amplifier. A similar approach was used in [33], where an implementation of an all-digital Signal Component Separator (SCS) with branch mismatch compensation was presented.

This paper presents a model-based phase-only predistortion method suitable for outphasing RF PAs. The predistortion method is based on a model of the amplifier with a constant gain factor and phase rotation for each outphasing signal, and a predistorter with phase rotation only. The predistorter proposed

Manuscript received June 26, 2012; revised September 27, 2012; accepted October 21, 2012. This work has been supported by the Excellence Center at Linköping-Lund in Information Technology (ELLIIT), the Swedish Research Council (VR), and Ericsson Research, Kista, Sweden.

Y. Jung, M. Enqvist, and A. Alvandpour are with the Department of Electrical Engineering, Linköping University, SE-581 83 Linköping, Sweden, phone: +46(0)13-284474, e-mail: ylvju@isy.liu.se, maren@isy.liu.se, atila@isy.liu.se.

J. Fritzin was with the Department of Electrical Engineering, Linköping University, SE-581 83 Linköping, Sweden. He is now with Ericsson AB, SE-164 80 Stockholm, Sweden, e-mail: jonas@jonasfritzin.com.

in this paper compensates for both amplitude and phase distortion by changing only the phases of the two input outphasing signals, and thus a second voltage supply is not needed to compensate for the gain mismatch. By making use of the specific structure of outphasing PAs, the model estimation can be reformulated from a nonconvex problem into a convex least-squares problem, and the predistorter can be calculated analytically, thus making iterations like in [16] unnecessary. The solution in [33] considers the gain mismatch between the two branches and computes the ideal phase compensation when the outputs are approximated as two constant amplitudes. This is possible when there is no interaction between the amplifier stages, e.g. by using a combiner with isolation. In this paper, we also consider the outputs as two constant amplitudes generating amplitude and phase distortion, (14)-(16), but the amplitude dependent phase distortion that occurs due to the interaction and signal combining of the amplifiers' outputs is also considered. Thus, the approach in this paper includes another degree of distortion and the nonlinearities are used to create a linear least-squares predistortion method. A similar approach to the one in [16] is presented in [34], with suggestions on how to find good initial values for the nonlinear optimization needed to extract the model and DPD parameters. However, the basic problem of nonconvexity has not been solved in [16], [34] and local minima still risk posing problems in the optimization. For PVT variations or load impedance variations (as in handheld applications) our method can also be made adaptive, without significantly increasing the complexity as our method is a linear least-squares DPD method with a single optimal solution.

The proposed predistortion method has been used for WCDMA and LTE uplink signals with PAPR of 3.5 dB and 6.2 dB, respectively, applied to a fully integrated +30 dBm Class-D outphasing RF PA in 65nm CMOS [15], which is also one of the first fully integrated +30 dBm outphasing PAs [11], [14], [15]. The predistortion method was applied at the baseband level and has not been implemented in hardware. Implementing the proposed method involves many considerations, and as concluded in [25], "different methodologies or implementation structures will lead to very different results in terms of complexity and cost from the viewpoint of hardware implementation". Therefore, the purpose of the paper is to theoretically and practically demonstrate the capability of the proposed DPD method and describe it such that it can serve as a basis for hardware implementation. The evaluation criterion of the predistortion method is based on the measured ACLR, as Error Vector Magnitude (EVM) requirements were easily met without predistortion [15].

The outline of the paper is as follows. In Section II, the outphasing concept is explained mathematically. In Section III, an ideal phase predistorter is described, and the implementation of a DPD estimator is shown in Section IV, followed in Section V by a discussion on benefits with the least-squares formulation presented here. The impact of PVT variations and dynamic range is discussed in Section VI and the PA used in the measurements is described in Section VII. In Section VIII, the measured RF performance and the performance for modulated signals with and without phase-predistortion are presented. In Section IX, the conclusions are provided.

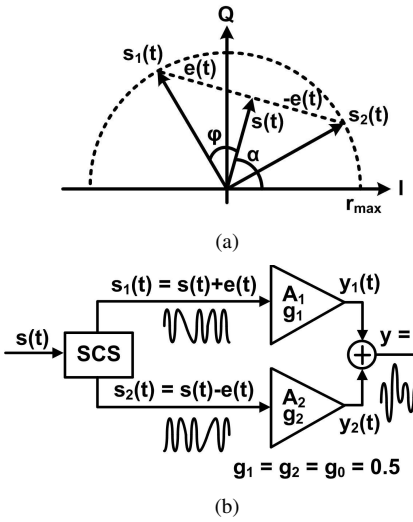

Fig. 1. (a) Outphasing concept and signal decomposition. (b) Ideal power combining of the two constant-envelope signals, where the amplitude of the output is normalized to 1.

II. Outphasing Concept

The outphasing concept is shown in Fig. 1(a), where a non-constant envelope-modulated signal

$$s(t) = r(t)e^{j\alpha(t)} = r_{\max}\cos(\varphi(t))e^{j\alpha(t)}, 0 \le r(t) \le r_{\max} \quad (1)$$

where $r_{\max}$ is a real-valued constant, is used to create two constant-envelope signals, $s_1(t)$ and $s_2(t)$, in the SCS in Fig. 1(b) as

$$\begin{aligned} s_1(t) &= s(t) + e(t) = r_{\max}e^{j\alpha(t)}e^{j\varphi(t)} \\ s_2(t) &= s(t) - e(t) = r_{\max}e^{j\alpha(t)}e^{-j\varphi(t)} \\ e(t) &= js(t)\sqrt{\frac{r_{\max}^2}{r^2(t)} - 1}. \end{aligned} \quad (2)$$

The signals $s_1(t)$ and $s_2(t)$, contain the original signal, $s(t)$, and a quadrature signal, $e(t)$, and are suitably amplified by switched amplifiers like Class-D/E. By separately amplifying the two constant-envelope signals and combining the outputs of the two individual amplifiers as in Fig. 1(b), the output signal is an amplified replica of the input signal. In the sequel, PA refers to the complete outphasing amplifier and amplifier refers to the switched amplifiers A_1 and A_2.

Letting g_1 and g_2 denote two positive real valued gain factors, on $s_1(t)$ and $s_2(t)$, and δ denote a phase mismatch in the path for $s_1(t)$, it is clear from

$$\begin{aligned} y(t) &= g_1e^{j\delta}s_1(t) + g_2s_2(t) \\ &= [g_1e^{j\delta} + g_2]s(t) + [g_1e^{j\delta} - g_2]e(t), \end{aligned} \quad (3)$$

that besides the amplified signal, a part of the quadrature signal remains. As the bandwidth of the quadrature signal is larger than the original signal, $s(t)$, the ACLR is degraded and the margins to the spectral mask are reduced, unless the quadrature signals are canceled in the power combiner [5], [21]. The phase and gain mismatches between $s_1(t)$ and $s_2(t)$

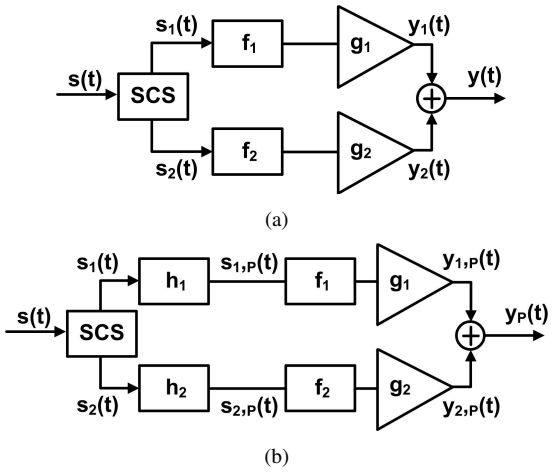

Fig. 2. A schematic picture of (a) the amplifier branches setup and (b) the amplifiers with predistorters. Note that the functions f_k and h_k, $k = 1, 2$, are not functions of the input to the block only but are used to show the general functionality of the PA and the DPD with the separation of the two branches.

must be minimized in order not to allow a residual quadrature component to distort the spectrum or limit the Dynamic Range (DR)

$$c_{DR} = 20\,\log_{10}\left(\frac{\max(|y(t)|)}{\min(|y(t)|)}\right) = 20\,\log_{10}\left(\frac{|g_1+g_2|}{|g_1-g_2|}\right) \tag{4}$$

of the PA [5]. While the DR defines the ratio of the maximum and minimum output amplitudes the PA can achieve, all amplitudes and phases within the DR can be reached by changing the phases of the outphasing signals. As the output of a Class-D stage can be considered as an ideal voltage source whose output voltage is independent of the load [17], i.e. the output is connected to either V_{DD} or *GND*, the constant gain approximations g_1 and g_2 are appropriate and make Class-D amplifiers suitable for non-isolating combiners like transformers [11]–[16].

III. Amplifier and predistorter modeling

A physical outphasing PA differs from the ideal PA in more ways than the constant gain and phase mismatches described in the previous section. Initial tests with the PA have shown a phase distortion on the output that seems to depend on the amplitude of the input $s(t)$. Based on this observation, a mathematical description of the physical outphasing PA has been formulated and a digital predistorter (DPD) has been proposed. Since it is desired that the predistorter should invert all effects of the PA except for the gain, the signals are assumed to be normalized such that

$$\max_t |s(t)| = \max_t |y(t)| = 1. \tag{5}$$

Despite the fact that the PA is analog and the baseband model is time-discrete, the notation t is used for indicating the dependency of time. Based on the context, t may thus be a continuous or discrete quantity and denote the time or the time indexation. For notational convenience, the explicit dependency on time will be omitted in parts of this section and the following one.

Parts of the results in this section were presented in [16] but are restated here for sake of completeness. In [16], the results were merely used for motivation and evaluation purposes, whereas they are here part of the algorithm to obtain the predistorter, as shown later in Section IV. The new contribution is the reformulation of the nonconvex modeling problem to a convex problem, thus guaranteeing that the global minimum will be found in the optimization.

In this section, the setup is explained and the ideal predistorter is described. This will be followed by a description of how a DPD can be estimated in practice, in the next section.

A. PA and DPD description

Let

$$\Delta_\psi(s_1, s_2) = \arg(s_1) - \arg(s_2) \tag{6}$$

denote the phase difference of the outphasing signals $s_1(t)$ and $s_2(t)$. Since the amplitude of the nondecomposed signal in the outphasing system is determined by $\Delta_\psi(s_1, s_2)$, this difference can be used instead of the actual amplitude in many cases. For notational convenience, Δ_ψ will be used instead of $\Delta_\psi(s_1, s_2)$, unless specified otherwise. Here, all phases are assumed unwrapped.

A description of the amplitude-dependent phase distortion in $y_k(t), k = 1, 2$ (the two amplifier branches) can be done as

$$y_k(t) = g_k e^{j\,f_k(\Delta_\psi)} s_k(t), \quad k = 1, 2, \tag{7a}$$

$$y(t) = y_1(t) + y_2(t), \tag{7b}$$

in case there is no DPD in the system as in Fig. 2(a). Here, f_1 and f_2 are two real-valued functions describing the phase distortion

$$\arg(y_k) - \arg(s_k) = f_k(\Delta_\psi), \quad k = 1, 2, \tag{8}$$

in each signal path. Furthermore, g_1 and g_2 are the gain factors in each amplifier branch. The normalization (5) implies that $g_1 + g_2 = 1$. Hence, an ideal PA would have $f_1 = f_2 = 0$ and $g_1 = g_2 = g_0 = 0.5$ and any deviations from these values will cause non-linearities in the output signal and spectral distortion as previously concluded. In order to compensate for these effects, a DPD can be used to modify the input outphasing signals, i.e. $s_1(t)$ and $s_2(t)$, to the two amplifier branches.

Since the outputs of the Class-D stages have constant envelopes, the DPD may only change the phase characteristics of the two input outphasing signals. With this in mind, a DPD that produces the predistorted signals

$$s_{k,P}(t) = e^{j\,h_k(\Delta_\psi)} s_k(t), \quad k = 1, 2, \tag{9}$$

to the two amplifier branches is proposed. Here, h_1 and h_2 are two-real-valued functions that depend on the phase difference between the two signal paths. By modifying the signals in each branch using the DPD in (9) as shown in Fig. 2(b), the PA output $y_P(t)$ can be written

$$y_P = \underbrace{g_1 e^{j\,f_1(\Delta_\psi(s_{1,P}, s_{2,P}))} s_{1,P}}_{\triangleq y_{1,P}} + \underbrace{g_2 e^{j\,f_2(\Delta_\psi(s_{1,P}, s_{2,P}))} s_{2,P}}_{\triangleq y_{2,P}}. \tag{10}$$

The phase difference between the two paths after the predistorters is described by

$$\begin{aligned}\Delta_\psi(s_{1,P}, s_{2,P}) &= \arg(s_{1,P}) - \arg(s_{2,P}) \\ &= [\arg(s_1) + h_1(\Delta_\psi)] \\ &\quad - [\arg(s_2) + h_2(\Delta_\psi)] \\ &= \Delta_\psi + h_1(\Delta_\psi) - h_2(\Delta_\psi) \triangleq \tilde{h}(\Delta_\psi) \quad (11)\end{aligned}$$

and the phase difference between the two paths at the (predistorted) outputs by

$$\begin{aligned}\Delta_\psi(y_{1,P}, y_{2,P}) &= \arg(y_{1,P}) - \arg(y_{2,P}) = \\ &= [\arg(s_{1,P}) + f_1(\Delta_\psi(s_{1,P}, s_{2,P}))] \\ &\quad - [\arg(s_{2,P}) + f_2(\Delta_\psi(s_{1,P}, s_{2,P}))] \\ &= \Big[\arg(s_1) + h_1(\Delta_\psi) + f_1(\tilde{h}(\Delta_\psi))\Big] \\ &\quad - \Big[\arg(s_2) + h_2(\Delta_\psi) + f_2(\tilde{h}(\Delta_\psi))\Big] \\ &= \Delta_\psi + h_1(\Delta_\psi) - h_2(\Delta_\psi) \\ &\quad + f_1(\tilde{h}(\Delta_\psi)) - f_2(\tilde{h}(\Delta_\psi)) \\ &= \tilde{h}(\Delta_\psi) + f_1(\tilde{h}(\Delta_\psi)) - f_2(\tilde{h}(\Delta_\psi)) \\ &\triangleq \tilde{f}(\tilde{h}(\Delta_\psi)). \quad (12)\end{aligned}$$

Thus, the absolute phase change in each branch is given by

$$\arg(y_{k,P}) = \arg(s_k) + h_k(\Delta_\psi) + f_k(\Delta_\psi(s_{1,P}, s_{2,P})) \quad (13)$$

for $k = 1, 2$.

B. The ideal DPD

As mentioned above, the PA output signal $y(t)$ is a distorted version of the input signal. An ideal DPD should compensate for this distortion and result in a normalized output signal $y_P(t) = y_{1,P}(t) + y_{2,P}(t)$ that is equal to the input signal $s(t) = 0.5s_1(t) + 0.5s_2(t)$. In the ideal case when $g_1 = g_2 = g_0 = 0.5$, this is obtained when $y_1(t) = 0.5s_1(t)$ and $y_2(t) = 0.5s_2(t)$. However, this is not possible to achieve when $g_k \neq 0.5, k = 1, 2$.

In this case, the ideal values for $y_{1,P}(t)$ and $y_{2,P}(t)$ are instead $\tilde{s}_1(t)$ and $\tilde{s}_2(t)$, respectively. These signals define an alternative decomposition of $s(t)$ such that

$$\tilde{s}_1(t) + \tilde{s}_2(t) = s(t), \quad (14a)$$

$$|\tilde{s}_k| = g_k, \quad k = 1, 2, \quad \text{and} \quad (14b)$$

$$\arg(\tilde{s}_1) \geq \arg(\tilde{s}_2). \quad (14c)$$

Given g_1, $g_2 = 1 - g_1$ and $s(t)$, the signals $\tilde{s}_1(t)$ and $\tilde{s}_2(t)$ can be computed from (14). Let

$$b_1 = \arg(\tilde{s}_1) - \arg(s)$$

and

$$b_2 = \arg(s) - \arg(\tilde{s}_2)$$

denote the angles between the decomposed signals and $s(t)$ as shown in Fig. 3(a). Fig. 3(b) shows that the decomposition can be viewed as a trigonometric problem and application of the law of cosines gives

$$g_2^2 = g_1^2 + |s|^2 - 2g_1|s|\cos(b_1) \quad (15)$$

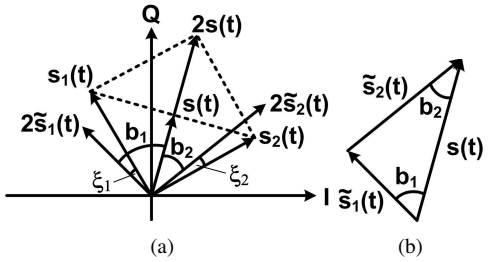

Fig. 3. (a) Decomposition of the input signal $s(t)$ into $s_1(t)$ and $s_2(t)$ when $g_1 = g_2 = g_0 = 0.5$ and into $\tilde{s}_1(t)$ and $\tilde{s}_2(t)$ when decomposed as in (14) with nonidentical gain factors g_1 and g_2. (b) Trigonometric view of the decomposition of $s(t)$ using nonidentical gain factors. Note that $|\tilde{s}_k| = g_k, k = 1, 2$.

and

$$g_1^2 = g_2^2 + |s|^2 - 2g_2|s|\cos(b_2). \quad (16)$$

The angles b_1 and b_2 that define $\tilde{s}_1(t)$ and $\tilde{s}_2(t)$ can be computed from these expressions and can be viewed as functions of Δ_ψ since $|s|$ is a function of Δ_ψ. This implies that the angles

$$\xi_1(\Delta_\psi) \triangleq \arg(\tilde{s}_1) - \arg(s_1) = b_1 - \frac{1}{2}\Delta_\psi \quad (17)$$

and

$$\xi_2(\Delta_\psi) \triangleq \arg(\tilde{s}_2) - \arg(s_2) = \frac{1}{2}\Delta_\psi - b_2 \quad (18)$$

can also be viewed as functions of Δ_ψ.

Assume that an ideal DPD (9) is used together with the PA (7). In this case, the equalities

$$y_{1,P}(t) = \tilde{s}_1(t) \quad (19)$$

and

$$y_{2,P}(t) = \tilde{s}_2(t) \quad (20)$$

hold, which results in

$$y_P(t) = y_{1,P}(t) + y_{2,P}(t) = \tilde{s}_1(t) + \tilde{s}_2(t) = s(t).$$

In particular, in order not to change the amplitude at the output, the phase difference between $y_{1,P}(t)$ and $y_{2,P}(t)$ must be equal to the one between $\tilde{s}_1(t)$ and $\tilde{s}_2(t)$, i.e.,

$$\begin{aligned}\Delta_\psi(y_{1,P}, y_{2,P}) &= \arg(\tilde{s}_1) - \arg(\tilde{s}_2) = \\ &= [\arg(s_1) + \xi_1(\Delta_\psi)] - [\arg(s_2) + \xi_2(\Delta_\psi)] \\ &= \Delta_\psi + \xi_1(\Delta_\psi) - \xi_2(\Delta_\psi) \triangleq \tilde{\xi}(\Delta_\psi). \quad (21)\end{aligned}$$

Hence, inserting (21) into (12) gives

$$\tilde{f}(\tilde{h}(\Delta_\psi)) = \tilde{\xi}(\Delta_\psi) \quad \Leftrightarrow \quad \tilde{h}(\Delta_\psi) = \tilde{f}^{-1}(\tilde{\xi}(\Delta_\psi)), \quad (22)$$

assuming that $\tilde{f}$ is invertible. Furthermore, for (19) and (20) to hold, we require

$$\arg(y_{k,P}) = \arg(\tilde{s}_k), \quad k = 1, 2.$$

Combined with (11), (13) and (17) or (18), respectively, this gives

$$\arg(s_k) + h_k(\Delta_\psi) + f_k(\tilde{h}(\Delta_\psi)) = \arg(s_k) + \xi_k(\Delta_\psi), \; k = 1, 2,$$

which results in

$$\begin{aligned} h_k(\Delta_\psi) &= -f_k(\tilde{h}(\Delta_\psi)) + \xi_k(\Delta_\psi) \\ &= -f_k(\tilde{f}^{-1}(\tilde{\xi}(\Delta_\psi))) + \xi_k(\Delta_\psi) \end{aligned} \tag{23}$$

for $k = 1, 2$. Here, (22) has been used in the last equality.

Hence, using the predistorters (23) as in (9), the output $y(t)$ will be an amplified replica of the input signal $s(t)$, despite the gain mismatch and nonlinear behavior of the amplifiers.

IV. A Least-squares DPD estimator

The ideal predistorter requires the unknown characteristics g_1, g_2, f_1 and f_2 of the PA, which have to be estimated from a sequence of input and output measurements referred to as estimation data. In [16], a model of the PA was estimated by minimizing a quadratic cost function measuring the difference between the measured and predicted output signal. Based on this model, the DPD was estimated in a second step by minimizing a similar cost function measuring the difference between $s(t)$ and the predicted, precompensated output $y_P(t)$. Both these estimation problems involve solving a nonconvex optimization problem, which might be a challenging task due to the presence of local minima. However, using the mathematical characterization of the DPD and PA derived here, there is an alternative way which essentially only involves solving standard least-squares problems.

Consider first the two gain factors g_1 and $g_2 = 1 - g_1$, where the relation between them comes from the normalization (5). Let

$$\begin{aligned} g_1 &= g_0 \pm \Delta_g, \\ g_2 &= g_0 \mp \Delta_g, \end{aligned} \tag{24}$$

where $\Delta_g \geq 0$ represents the gain imbalance between the amplifier stages and $g_0 = 0.5$. Inserting (24) into (4) gives

$$c_{DR} = 20 \log_{10}\left(\frac{g_0}{\Delta_g}\right). \tag{25}$$

Hence, the imbalance term Δ_g can be computed as

$$\Delta_g = g_0 \cdot 10^{-c_{DR}/20}, \tag{26}$$

making it possible to find approximations of g_1 and g_2 from the dynamic range of the output signal. The value of c_{DR} can be estimated from measurements as the ratio between the maximum and minimum output amplitudes. This estimate is noise sensitive, but this can be handled by averaging multiple realizations. These approximations are valid for input signals with large peak to minimum power ratios, like WCDMA and LTE, where the PA generate an output signal including its peak and minimum output amplitudes (i.e. its full dynamic range). If this is not fulfilled or the noise influence is too large, an alternative to this approach is to evaluate a range of values of g_1 and $g_2 = 1 - g_1$ and then solve the PA modeling problem for each pair of gain factors.

Once the gain factors have been determined, $s(t)$ can be decomposed into $\tilde{s}_1(t)$ and $\tilde{s}_2(t)$ using (14) to (16). Furthermore, the standard outphasing decomposition of $s(t)$ into $s_1(t)$ and $s_2(t)$ as in (2) will be used in the sequel.

The distortions originate both from imperfect gain factors and nonlinearities in the amplifiers. Once the gain factor impact has been accounted for, the amplifier nonlinearities can be modeled. Since the gain factors are now assumed known, the output can be decomposed into $y_1(t)$ and $y_2(t)$ in the same way as $s(t)$ is decomposed into $\tilde{s}_1(t)$ and $\tilde{s}_2(t)$. The remaining output distortion is due to the nonlinearities in the path from $\tilde{s}_k(t)$ to $y_k(t), k = 1, 2$.

The phase distortion in each signal path caused by the amplifiers can thus be modeled from measurements of $s(t)$ and $y(t)$. Here, polynomials

$$p(\eta_k, \Delta_\psi) = \sum_{i=0}^{n} \eta_{k,i} \Delta_\psi^i, \quad k = 1, 2, \tag{27}$$

have been used as parameterized versions of the functions f_k, motivated by the Stone-Weierstrass theorem (Theorem 7.26 in [35]). Estimates $\hat{\eta}_{k,i}$ of the model parameters $\eta_{k,i}$ have been computed by minimizing quadratic cost functions, i.e.,

$$\hat{\eta}_k = \arg\min_{\eta_k} V_k(\eta_k), \quad k = 1, 2, \tag{28}$$

where

$$\begin{aligned} &V_k(\eta_k) \\ &= \sum_{t=1}^{N} (\arg(y_k(t)) - \arg(s_k(t)) - p(\eta_k, \Delta_\psi(s_1(t), s_2(t))))^2, \end{aligned} \tag{29}$$

and

$$\eta_k = \begin{pmatrix} \eta_{k,0} & \eta_{k,1} \dots & \eta_{k,n} \end{pmatrix}^T.$$

The cost function (29) can be motivated by the fact that the true functions f_k satisfy (8) when the amplifier is described by (7). Minimization of V_1 and V_2 are standard least-squares problems, which guarantees that the global minimum will be found [36].

Once the LS problem is solved for each setup of g_1 and g_2, the problem of finding the best setup is now reduced to a one dimensional (possibly nonconvex) optimization problem over $g_1 (g_2 = 1 - g_1)$, wich is much easier to solve than the original, multidimensional problem. A problem this small can be solved at a small computational cost by a global optimization method such as parameter gridding.

The parameter estimates $\hat{\eta}_k$ define function estimates

$$\hat{f}_k(z) = p(\hat{\eta}_k, z), \quad k = 1, 2, \tag{30}$$

from which an estimate

$$\hat{\tilde{f}}(z) = z + \hat{f}_1(z) - \hat{f}_2(z) \tag{31}$$

of the function $\tilde{f}$ from (12) can be computed. Provided that this function can be inverted numerically, estimates $\hat{h}_k$ of the ideal phase correction functions can be computed as in (23), i.e.,

$$\hat{h}_k(\Delta_\psi) = -\hat{f}_k(\hat{\tilde{f}}^{-1}(\tilde{\xi}(\Delta_\psi))) + \xi_k(\Delta_\psi) \tag{32}$$

for $k = 1, 2$, where Δ_ψ is given by (6) and $\tilde{\xi}$, ξ_1 and ξ_2 by (21), (17) and (18), respectively.

Hence, the complete DPD estimator consists of the selection of gain factors g_1 and g_2, the two least-squares estimators

given by (28), a numerical function inversion in order to obtain $\hat{\tilde{f}}^{-1}$ and the expressions for the phase correction functions in (32). The DPD estimation can either be done at each point in time, or (as has been done here) by evaluating the function for the range of possible Δ_ψ and saving this nonparametric, piecewise constant function.

The DPD estimator will result in two functions $\hat{h}_1$ and $\hat{h}_2$ which take Δ_ψ as input, and by using these as in (9), the predistorted input signals $s_{1,P}(t)$ and $s_{2,P}(t)$ can be calculated for arbitrary data. The measured results for a new data set, validation data, not used during the modeling, are presented in Section VIII.

The algorithm thus consists of two main parts, A – Estimation of PA model and B – Calculation of DPD functions. Part A consists of three parts where the first, A.I, produces candidates for the gain factors g_1 and g_2 by either using the DR or by gridding the possible values. A.II produces LS estimates of the nonlinear functions $\hat{f}_1$ and $\hat{f}_2$ for each pair of g_1 and g_2 and in A.III, the best performing model is chosen among all the candidates. In Part B, the DPD functions $\hat{h}_1$ and $\hat{h}_2$ are calculated. The different steps are described in more detail in Algorithm 1.

V. Benefits of the Least-squares DPD estimator

A. Convex and Nonconvex Formulations

The minimization of the cost function (9)-(10) in [16],

$$\hat{\theta} = \arg\min_{\theta} \sum_{t=1}^{N} |y(t) - \hat{y}(t,\theta)|^2 \tag{33}$$
$$\hat{y}(t,\theta) = g_1 e^{j\, p(\eta_1,\Delta_\psi)} s_1(t) + g_2 e^{j\, p(\eta_2,\Delta_\psi)} s_2(t)$$

where $\theta = [g_1 \quad g_2 \quad \eta_1^T \quad \eta_2^T]^T$, $y(t)$ is the measured output data and $\hat{y}(t)$ is the modeled output, is a nonconvex optimization problem in $2n+4$ dimensions with possible presence of local minima. Nonconvex optimization problems can either be solved by a local optimization method or a global one. A local optimization method minimizes the cost function over points close to the initial point, and guarantees convergence to a local minimum only. Global methods find the global minimum, at the expense of efficiency [37]. Hence, even under ideal conditions (noise-free data, true PA described exactly by one model with the proposed structure), there is no guarantee that the previous non-convex approach (33) will produce an optimal model of the PA in finite time, whereas the new least-squares approach does exactly this and results in a closed-form expression for the parameter estimate. This is a major advantage since it removes the need for error-prone sub-optimality tests and possible time-consuming restarts of the search algorithm. Additionally, the computation time for the iterative, non-convex, and potentially sub-optimal solution is significantly longer than for the proposed least-squares method.

A two dimensional projection of the cost functions to be minimized, (33) in the nonlinear formulation and (29) in the LS reformulation, can be seen in Fig. 4. The WCDMA signal used is described in more detail in Section VIII. All parameters but two have been fixed at the optimum, and the linear term in

Algorithm 1 LS DPD method

Require: model order n, method for choice of g_1 and g_2, precision of PA model (p_M) and inverse (p_I), estimation data.

{**A – Estimation of PA model**}

1: Normalize the output $y(t) = \frac{y(t)}{max(|y(t)|)}$
2: Calculate $\Delta_\psi\ \forall t$ according to (6).

{**A.I – Estimation of gain factor candidates g_1 and g_2**}

3: **if** Use Dynamic Range to determine g_1 and g_2 **then**
4: Calculate c_{DR} using (4), and Δ_g using (26).
5: Calculate possible choices of g_1, g_2 according to (24).
6: **else** {g_1 and g_2 over a range of values}
7: Grid $g_1 \in [g_{\min}, g_{\max}]$ with precision p_M and let $g_2 = 1 - g_1$.
8: **end if**

{**A.II – Estimation of nonlinearity function candidates $\hat{f}_1$ and $\hat{f}_2$**}

9: **for** all pairs of g_1, g_2 **do**
10: Create $\tilde{s}_k = g_k e^{j\ \arg(\tilde{s}_k)}$ and $y_k = g_k e^{j\ \arg(y_k)}, k = 1, 2$ using (15) to (18).
11: Find η_k using (28) and calculate $\hat{f}_k, k = 1, 2$ using (30).
12: Simulate the output $\hat{y}_{g_1,g_2}(t) = g_1 e^{j\,\hat{f}_1(\Delta_\psi)} s_1(t) + g_2 e^{j\,\hat{f}_2(\Delta_\psi)} s_2(t)$.
13: Calculate error $V_g(g_1, g_2) = \sum_t |y(t) - \hat{y}_{g_1,g_2}(t)|^2$.
14: **end for**

{**A.III – Choose best forward model, $\hat{g}_1, \hat{g}_2, \hat{f}_1$ and $\hat{f}_2$**}

15: Select $\hat{g}_1 = \arg\min_{g_1} V_g(g_1, 1-g_1),\ \hat{g}_2 = 1 - \hat{g}_1$ and the corresponding $\hat{f}_1$ and $\hat{f}_2$.

{**B – Calculation of DPD functions $\hat{h}_1$ and $\hat{h}_2$**}
{Create a Look Up Table (LUT) for different values of Δ_ψ by using an intermediate signal s.}

16: Grid $\Delta_\psi \in [0, \pi]$ with precision p_I.
17: **for** each value of Δ_ψ **do**
18: Create $s = \cos(\Delta_\psi/2)$ according to (1) assuming $\alpha = 0$ and $r_{\max} = 1$ ($\varphi = \frac{\Delta_\psi}{2}$).
19: Create s_1 and s_2 according to (2) and $\tilde{s}_1$ and $\tilde{s}_2$ using (14) to (16).
20: Find $\tilde{\xi}$ using (21), (17) and (18).
21: Calculate $\hat{\tilde{f}}(\tilde{\xi})$ using (31)
22: **end for**
23: Invert $\hat{\tilde{f}}(\tilde{\xi})$ numerically to get $\hat{\tilde{f}}^{-1}$. This can e.g. be done by calculating $\hat{\tilde{f}}(\tilde{\xi})$ for a number of values of $\tilde{\xi} \in [0, \pi]$, grid $\hat{\tilde{f}}(\tilde{\xi})$ and match with the $\tilde{\xi}$ that gives the closest value.
24: **for** each value of Δ_ψ in line 16 **do**
25: Find estimate $\hat{h}_k(\Delta_\psi)$ according to (32).
26: **end for**

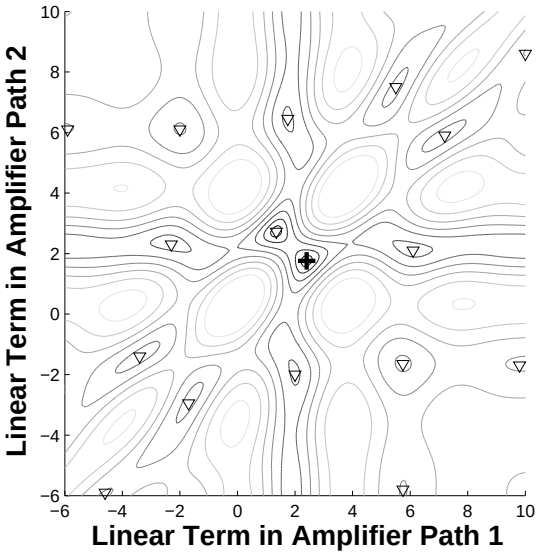

(a)

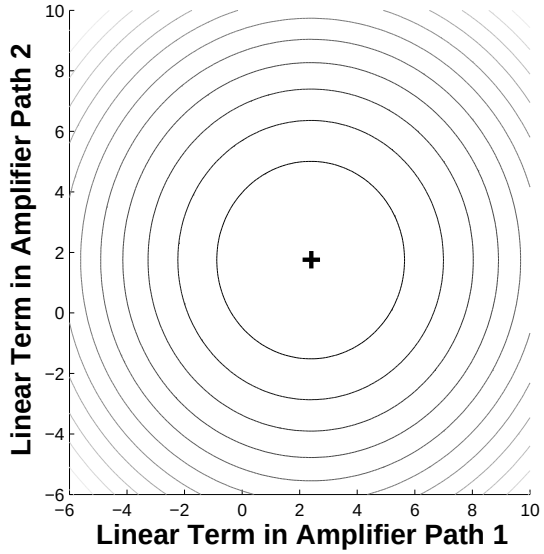

(b)

Fig. 4. Two dimensional projections of the cost functions of (a) the original nonconvex optimization problem and (b) the least-squares reformulation. All but two parameters in each amplifier branch have been fixed at the optimal value, and the linear terms ($\eta_{k,1}$ in (27)) are varied. In (a), the visible local minima are marked with $\bigtriangledown$ and the minimum obtained clearly depends on the initial point of the local optimization. In the least-squares formulation illustrated in (b), there is only one minimum (the global one) and convergence is guaranteed. The $+$ is the global minimum.

each amplifier branch ($\eta_{k,1}$ in (27)) has been varied. Clearly, there is a risk of finding a local minimum in the nonconvex formulation illustrated in (a) whereas there is only one (global) optimum in the least-squares formulation in (b).

The local minima in themselves might not be a problem if they are good enough to produce a wellperforming DPD, but there are no guarantees that this is the case. Typically, a number of different initial points need to be tested in order to get a reasonable performance.

B. Recursive Least-Squares and Least Mean Squares

In addition to the guaranteed convergence, the least-squares formulations also have the advantage that there are many efficient numerical methods to solve them, and they can be solved recursively [38] making them suitable for an online implementation. An even less complex parameter estimation algorithm is the Least Mean Square (LMS) method, which can make use of the linear regression structure of the optimization problem, developed here in equations (8) and (27). LMS has been used for RF PA linearization [39] and implemented in Field Programmable Gate Array (FPGA) technology, as shown in [40].

With a recursive implementation of the algorithm, it is even more important that the algorithm can be proved to converge to good values, as no monitoring of the performance should be necessary in order to be useful in practice. On the other hand, a nonconvex solution as in (33) is not suitable for online implementation since it cannot guarantee convergence to good enough minima. In an offline application, the possibility to restart the optimization could be added but, together with the lack of a bound on the number of iterations, this does not seem like a good solution for an online version. Using well explored methods like RLS or LMS would result in a low-complexity implementation, and though it is hard to judge the exact complexity of the iterative implementation that would be needed for the online version of nonconvex solution, it is clear that it would be very hard to find an simpler one than for the low-complexity LMS version of the new method.

One way to handle the PVT variations and changes in the setting, such as aging, would be to use a method with a forgetting factor, reducing the influence of older measurements [36]. The RLS and LMS solutions assume the changes in the operating conditions to be slow.

VI. ACLR over Dynamic Range and the Impact of PVT Variations

As previously explained, the result of the limited DR is that all amplitude and phase errors occurring outside the DR cannot be corrected for. The signal clipping in an outphasing PA occurs at small amplitudes, while peak amplitudes in a conventional linear PA are clipped. Thus, the DR in an outphasing PA limits the spectral performance when amplifying modulated signals.

To investigate the performance limits of the predistorter, simulations have been done using two amplifiers with a given DR (no phase distortion), with and without DPD. In Fig. 5 the ACLR over DR at 5 MHz and 10 MHz for the WCDMA signal are plotted with DPD (solid line) and without (dashed line). In Fig. 6 the ACLR over DR at 5 MHz for the LTE signal are plotted with DPD (solid line) and without (dashed). In the figures, the phase error between the outphasing signals is assumed to be zero as this can be compensated for in the baseband. For a PA with a DR of 25 dB the differences in ACLR between the nonpredistorted and predistorted output

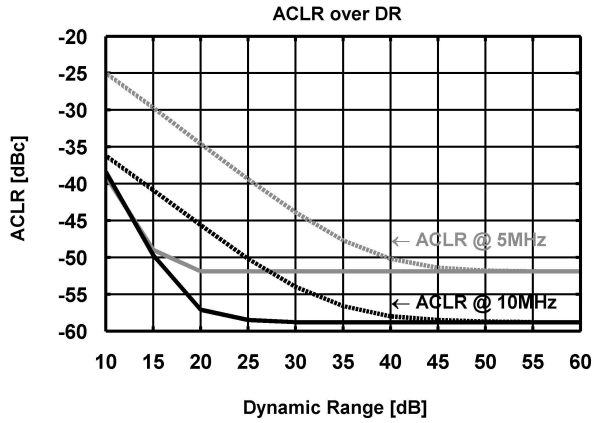

Fig. 5. Simulated ACLR at 5 MHz and 10 MHz offset with DPD (solid line) and without (dashed line) for the WCDMA signal.

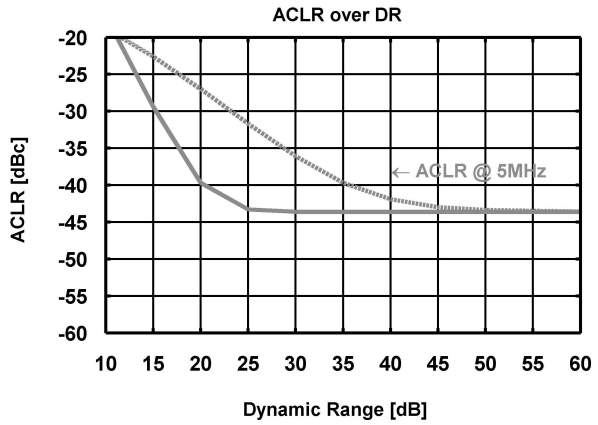

Fig. 6. Simulated ACLR at 5 MHz offset with DPD (solid line) and without (dashed line) for the 5 MHz LTE signal.

is 7.5-13 dB. When the DR is 25 dB the optimal theoretical ACLR is achieved after DPD. For a PA with 45 dB of DR the difference is negligible.

Changing the process corner (in simulations) from the nominal corner to all other process corners, the DR is, at worst, reduced by 2.5 dB. Similarly, varying the temperature from 25 to 125 degrees, the DR does vary by 2.5 dB. Combining the choice of process corner and temperature, the DR can be reduced up to 3.5 dB. As seen in Fig. 5 and Fig. 6, a variation of 3.5 dB in DR, the ACLR is degraded by approximately the same amount (here considering the case without DPD). If the supply voltage is varied, the DR in the output stage may vary as in Fig. 11(c) and may have an effect on how much of the distortion can be compensated for and also how much distortion can be expected without any DPD.

A. Dynamic Range Improvement by DC Bias Adjustment

In [41] a pulse-width and pulse-positioning method was described for a Class-E PA. Similarly, the amplitudes of the outphasing signals can be changed by changing the DC bias levels, V_{BIAS}, at the inputs of the Class-D stages as in Fig. 7(a), which are driven by the sinusoidal RF signal, v_{RF}. By changing the DC bias levels, the pulse widths and the associated duty

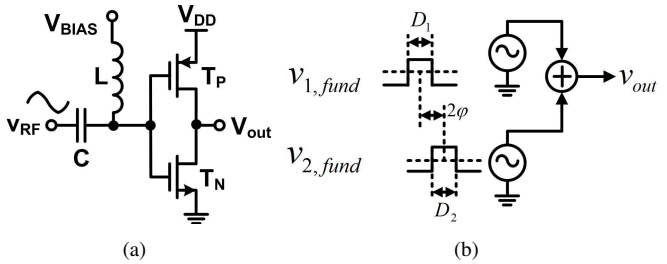

Fig. 7. (a) A Class-D stage with DC bias driven by a sinusoidal RF waveform. (b) Signal combining of the outputs of the Class-D stages and $s_1(t)$ and $s_2(t)$. The DC bias levels are adjusted to change the pulse width, D_1 and D_2, to change the amplitude of the fundamental tone.

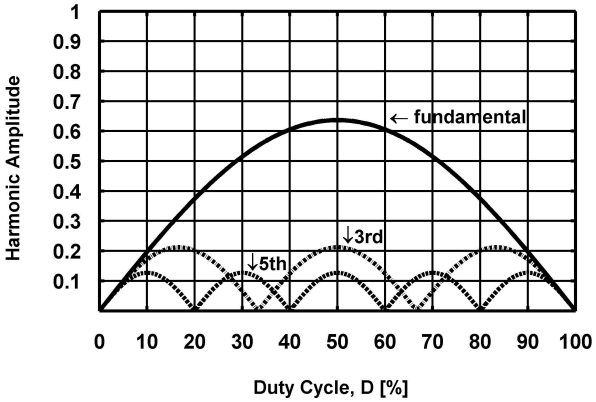

Fig. 8. Harmonic amplitude versus duty cycle, D.

cycles D_1 and D_2 of the output signal, V_{out}, of the Class-D stages are changed [42]. By changing the duty cycles, the corresponding amplitudes of the fundamental tone, $v_{1,\text{fund}}$ and $v_{2,\text{fund}}$, can be changed as illustrated in Fig. 7(b) and Fig. 8 and by (34).

$$v_{1,fund} = g_1 \frac{2V_{DD}}{\pi} \sin(\pi D_1) e^{j\varphi(t)}$$
$$v_{2,fund} = g_2 \frac{2V_{DD}}{\pi} \sin(\pi D_2) e^{-j\varphi(t)} \quad (34)$$

Thereby, the gain mismatch can be compensated for and the DR in the output stage can be improved. The only drawback of this method is that the peak output power is reduced as the pulse width of strongest signal is made larger (or smaller) to reduce the amplitude of the fundamental tone to compensate for the smaller amplitude of the other signal. This principle was used in measurements at 2.5 GHz for the measurement setup in Fig. 12, where the bias levels were adjusted to improve the DR from approximately 25 dB to 30 dB. The ACLR, before and after bias adjustment without DPD, was approximately -27 dBc and -32 dBc at an average output power of about +21 dBm for the LTE signal.

VII. Implementation of the Class-D Outphasing RF PA

Fig. 9 shows the implemented outphasing PA, based on a Class-D stage utilizing a cascode configuration illustrated in

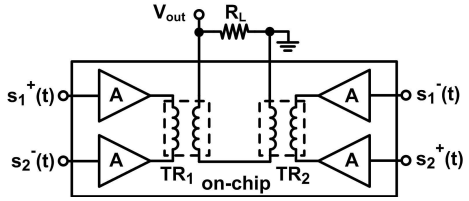

Fig. 9. The implemented Class-D outphasing RF PA using two transformers to combine the outputs of four amplifier stages. Chip photo in [15].

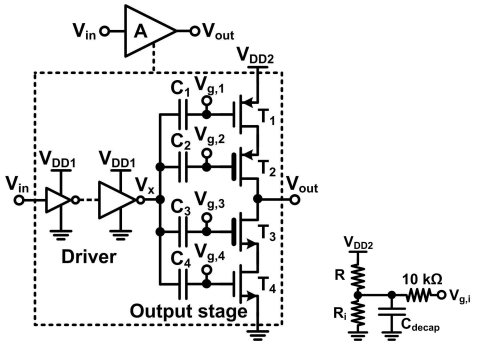

(a) (b)

Fig. 10. (a) The Class-D stage used in the outphasing PA [15]. C_1-C_4 are MIM capacitors. (b) Off-chip biasing resistors, R and R_i.

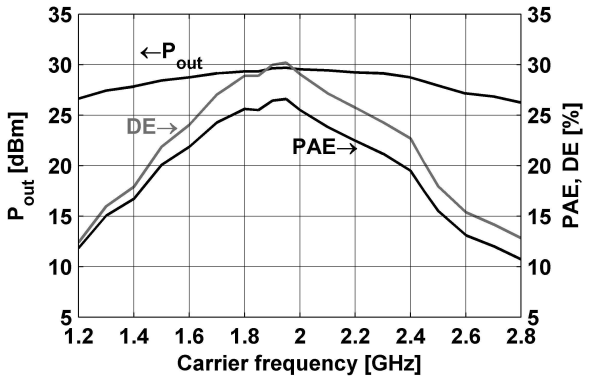

(a)

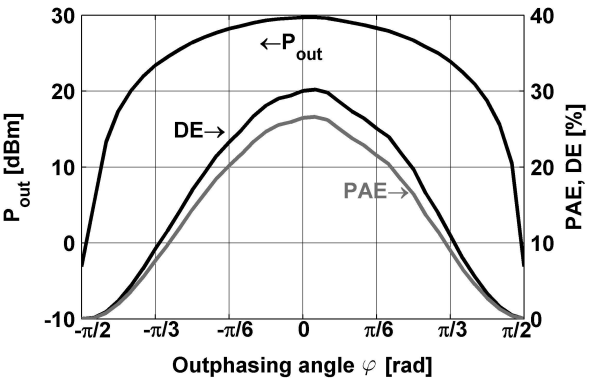

(b)

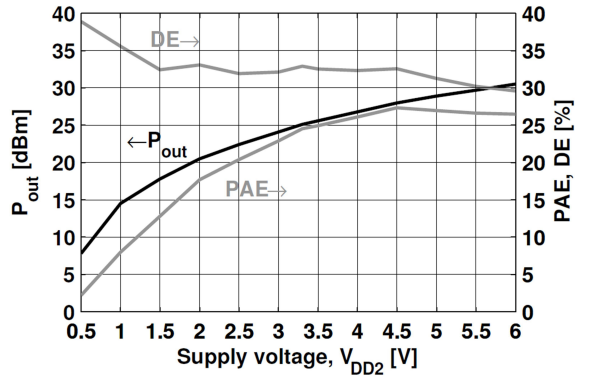

(c)

Fig. 11. Measured P_{out}, DE and PAE for V_{DD1} = 1.3 V and V_{DD2} = 5.5 V [15]:
(a) over carrier frequency.
(b) over outphasing angle, φ, at 1.95 GHz.
(c) Measured P_{out}, DE and PAE over V_{DD2} for V_{DD1} = 1.3 V at 1.95 GHz.

Fig. 10(a). The output stage is driven by an AC-coupled low-voltage driver operating at 1.3 V, V_{DD1}, to allow a 5.5 V, V_{DD2}, supply without excessive device voltage stress as discussed in [14], [15]. By driving all transistors in the cascode configuration it is possible to achieve a low on-resistance in the on-state, and distribute the voltage stress on the devices in the off-state, making sure that the root mean square (rms) electric fields across the gate oxide is kept low to improve the lifetime of the transistors [44]. This enables the use of a high supply voltage in the output stage to achieve an output power of +30 dBm [14], [15].

The four amplifier outputs are combined using two transformers, TR_1 and TR_2, where $s_1^+(t)$ and $s_2^-(t)$, and $s_1^-(t)$ and $s_2^+(t)$, are connected as described in [6]. In [6], the $s_1^+(t)$/$s_1^-(t)$ (and corresponding $s_2(t)$) signals were kept close to minimize parasitic differential ground inductance. With this connection, i.e. $s_1^+(t)$ and $s_2^-(t)$, and $s_1^-(t)$ and $s_2^+(t)$ connected to the primary windings of the transformers also used in this design, the matching network losses are reduced at power back-off. At zero output amplitude ($s_1^+(t) = s_2^-(t)$, $s_1^-(t) = s_2^+(t)$), the matching network losses are zero as the phase difference between the signals driving each individual transformer are zero. Thus, the load impedance is increased and the current through the load is reduced at power back-off and may help to improve efficiency as in [12]. To minimize AM-AM and AM-PM distortion, the left side of the layout of the outphasing PA is a mirrored version of the right side. Similarly, the PCB design is mirrored and off-chip baluns with small phase errors have been used. As the load is connected to one port of the equivalent secondary winding, consisting of the two series-connected transformers, and the second port is grounded, the signal combining is not perfectly symmetrical resulting in a small gain mismatch between the amplifier stages and AM-AM and AM-PM distortion.

On-chip resistors were used for an equivalent input impedance of 50 Ω at the chip edge for each of the RF inputs ($s_1^+(t)$, $s_1^-(t)$, $s_2^+(t)$, and $s_2^-(t)$). The chip photo of the PA implemented in a 65nm CMOS process is available in [15]. The chip was attached to an FR4 PCB and connected with bond-wires.

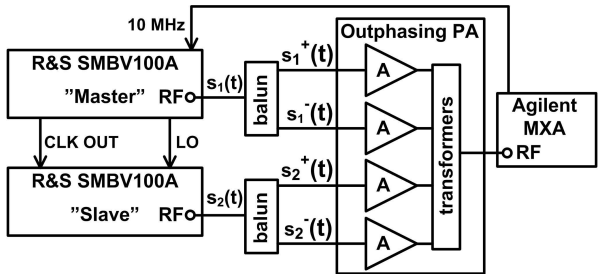

Fig. 12. Measurement setup for IQ data with two Master-Slave-configured SMBV signal generators [43].

VIII. Measurement Results

A. Measured RF Performance

Fig. 11(a) and Fig. 11(b) show the measured output power (P_{out}), drain efficiency (DE), and power-added efficiency (PAE) over frequency and outphasing angle, φ in (2), for V_{DD1} = 1.3 V and V_{DD2} = 5.5 V for the amplifier only. The predistortion method has not been implemented in hardware. At 1.95 GHz for a 5.5 V (6.0 V) supply voltage, the measured output power of the PA was +29.7 dBm (+30.5 dBm) with a power-added efficiency (PAE) of 27%. The PA had a peak to minimum power ratio of ∼35 dB. The gain was 26 dB from the drivers to the output. The DC power consumption of the smallest drivers was considered as input power.

The performance of the PA used in the measurements, denoted 'This PA', can be put in the context of published Class-D PAs as listed in Table I, sorted with regard to their output power.

Assuming that only the thin-gate oxide were driven by the driver and that the thick-gate oxide is held at the same bias level, the simulated DE and PAE, and output power were reduced about 15 % and 5 % and 0.5 dB relative the performance when all devices in the output stage are driven by the buffer. However, the rms gate-drain electrical fields in the oxide were increased by approximately 25 %, reducing the life-time of the oxide [44]. To have the same electrical fields as when all devices are driven by the buffer, the supply voltage had to be reduced to about 4 V, resulting in an output power reduction of ∼3 dB.

B. Measured Performance of Modulated Signals

The PAPR of the WCDMA and LTE uplink signals were 3.5 dB and 6.2 dB, respectively. The spectrum of the estimation data sets are shown in Fig. 15(c) and Fig. 16(c). Two R&S SMBV100A signal generators with phase-coherent RF outputs and arbitrary waveform generators with maximum IQ sample rate of 150 MHz, where $s_1(t)$ and $s_2(t)$ were stored, were used in the measurements. Fig. 12 shows the measurement setup. For the measurements without predistortion, the phase offset between $s_1(t)$ and $s_2(t)$ in the baseband was adjusted to minimize phase mismatch (ideally 0 ° between non-modulated $s_1(t)$ and $s_2(t)$, i.e. maximum output power for a continuous signal). Moreover, the IQ delay between the signal generators was adjusted for optimal performance [43].

Measurements with two amplitude-matched signal generators, i.e. $g_1 = g_2 = g_0 = 0.5$, show that phase errors of 12 ° and 7.5 ° are acceptable for WCDMA and LTE to meet the ACLR requirements. Thus, a predistortion implementation would require a phase resolution of at least 6 bits, i.e. $360\,^\circ/2^6 = 5.63\,^\circ$. For each bit of increased phase resolution, the ACLR improves by ∼3 dB.

TABLE I
Comparison of CMOS Class-D RF PAs - Peak Values

Ref. Year	P_{out} [dBm]	V_{DD} [V]	DE [%]	PAE [%]	f [GHz]	Tech. [nm]	BW [GHz]
[45] 2008	+20.0	2.4	-	38.5	2.40	90	0.3[b]
[19] 2007	+20.0	1.8	61.0	42.0	0.80	180	-
[20] 2010	+21.6	1.9	64.0	52.0	1.92	130	0.3[a]
[46], [47] 2010	+21.8	1.0	-	44.2	2.25	65	1.0[a]
[12] 2010	+25.1	2.0	-	40.6	2.40	32	1.0[a]
[48] 2011	+25.2	2.5	-	55.2	2.25	90	1.0[b]
[49] 2011	+25.2	3.0	-	45.0	2.25	90	1.0[b]
[6] 2011	+25.3	2.0	-	35.0	2.40	32	1.0[b]
[50] 2009	+28.1	2.4	-	19.7	2.25	45	0.6[b]
[15] 2011 This PA	**+29.7**	**5.5**	**30.2**	**26.6**	**1.95**	**65**	**1.6[b]**
[11] 2011	+31.5	2.4	-	27.0	2.40	45	1.7[b]
[14] 2011	+32.0	5.5	20.1	15.3	1.85	130	0.9[b]

(a) 1 dB and (b) 3 dB bandwidth (BW)

TABLE II
Data Collection

Standard	N_{id}	N_{val}	f_s	$f_{s,out}$	K
WCDMA	100 000	100 000	92.1 MHz	92.1 MHz	10
LTE	100 000	100 000	92.1 MHz	92.1 MHz	10

The estimation and validation data sets contain N_{id} and N_{val} samples, respectively. The input and output sampling frequencies are denoted f_s and $f_{s,out}$, respectively. To minimize the influence of measurement noise, the signals were measured K times, and a mean was calculated. The data collection parameters are shown in Table II.

An evaluation of the predistorter estimation can be seen in Fig. 13 for a model using the LTE input signal with polynomial degree $n = 5$. Here and in all following experiments, the DPD estimates $\hat{h}_k, k = 1, 2$, have been calculated for 3142 uniformly distributed points ($p_I = 0.001$ in Alg. 1). Ideally, the deviations from the ideal phase difference and the ideal phases in each branch should be zero, and (providing the PA model is good enough) it is clear that the predistorters reduce these deviations. Fig. 14 shows the measured AM/AM and AM/PM characteristics with DPD and without DPD for the LTE signal. The figure shows that the amplitude and phase errors are significantly reduced for small output amplitudes. The performance was similar for the WCDMA measurements.

For the WCDMA signal at 1.95 GHz without predistortion, the measured ACLR at 5 MHz and 10 MHz offsets were -35.5 dBc and -48.1 dBc, respectively. The spectrum is shown in Fig. 15(a). The estimation output data $y(t)$ were used in the predistortion method to extract the model parameters, with $n = 5$. The predistorted input signals, $s_{1,P}(t)$ and $s_{2,P}(t)$, were computed for the validation input signal, resulting in an output spectrum as shown in Fig. 15(b). The power spectral densities of the predistorted and the non-predistorted input outphasing signals are very similar and therefore not included in

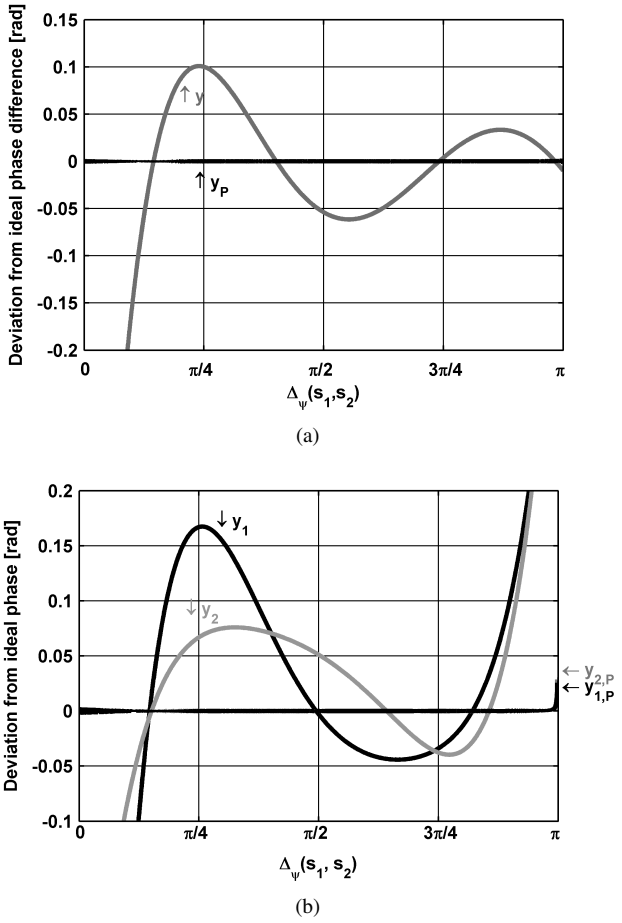

Fig. 13. Simulated predistorter evaluation for a model with polynomial degree $n = 5$ using the LTE input signal. The signals are generated using the PA model and the DPD estimator. (a) The deviation from the ideal phase difference without predistortion, y, and with predistortion, y_P. (b) The deviations from the ideal phase of the signals y_1 and y_2 without predistortion and with predistortion, $y_{1,P}$ and $y_{2,P}$.

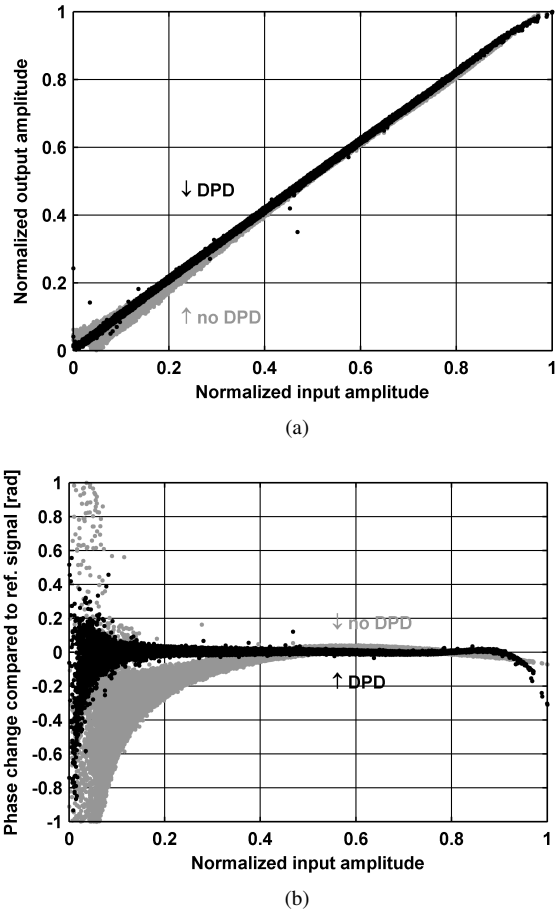

Fig. 14. (a) Measured AM/AM characteristics with DPD (black) and without DPD (grey) for LTE signal. (b) Measured AM/PM characteristics with DPD (black) and without DPD (grey) for LTE signal.

TABLE III
MEASURED SPECTRAL PERFORMANCE AT 1.95 GHZ FOR WCDMA AND LTE UPLINK SIGNALS WITH PREDISTORTION (USING $n = 5$) AND WITHOUT

Standard	Measured Parameter	W DPD	W/o DPD	Req
WCDMA	ACLR @ 5 MHz [dBc]	-46.3	-35.5	-33
	ACLR @ 10 MHz [dBc]	-55.6	-48.1	-43
LTE	ACLR @ 5 MHz [dBc]	-43.5	-34.1	-30

EVM requirements were easily met without predistortion for the WCDMA signal and an LTE signal (20 MHz, 16-QAM) without predistortion [15].

the paper (similarly for the LTE signal). With predistortion, the measured ACLR at 5 MHz and 10 MHz offsets were -46.3 dBc and -55.6 dBc, respectively. Thus, the measured ACLR at 5 MHz and at 10 MHz offsets were improved by 10.8 dB and 7.5 dB, respectively. The average power at 1.95 GHz was +26.0 dBm with 16.5 % PAE.

The receiver noise floor before and after predistortion, assuming a 45 MHz offset, was -127 dBc/Hz. Using two amplitude and phase matched signal generators with the outphasing signals, the noise level is the same. Thus, the noise level is limited by the signal generators, not the outphasing amplifier. The phase noise of a single signal generator was -140 dBc/Hz for a sinousoidal signal.

For the LTE signal at 1.95 GHz without predistortion, the measured ACLR at 5 MHz offset was -34.1 dBc. The spectrum is shown in Fig. 16(a). The estimation output data $y(t)$ were used in the predistortion method to extract the model parameters with $n = 5$. The predistorted input signals, $s_{1,P}(t)$ and $s_{2,P}(t)$, were computed for the validation input signal, resulting in an output spectrum as shown in Fig. 16(b). With the predistorted spectrum in Fig. 16(b), a small assymetry can be observed, which was expected due to the non-symmetrical frequency spectrum of the reference signal. With predistortion, the measured ACLR at 5 MHz offset was -43.5 dBc. Thus, the measured ACLR at 5 MHz offset was improved by 9.4 dB. The average power at 1.95 GHz was +23.3 dBm with 8.0 % PAE.

Fig. 17 shows the measured ACLR over the polynomial degree n of the PA model for the WCDMA and LTE signals. For each increase of order, the ACLR is improved by on average ∼2 dB. However, making the order larger than 5 does not significantly improve ACLR any further.

The measured performance of the PA for modulated signals is summarized in Table III. The table shows measured ACLR with DPD (W DPD), without DPD (W/o DPD), and the required (Req) ACLR for the WCDMA [51] and the LTE [52]

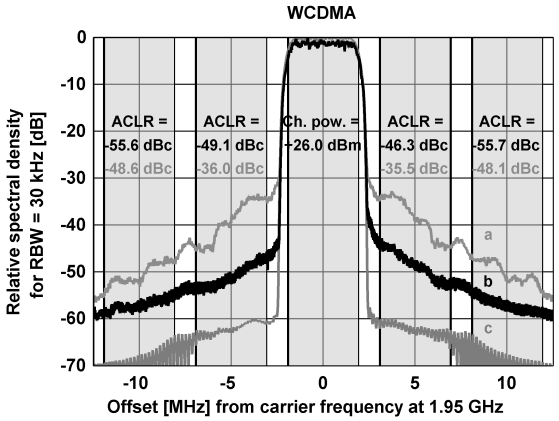

Fig. 15. Measured WCDMA spectrum at 1.95 GHz.
(a) Measured WCDMA spectrum without DPD. The measured ACLR is printed in grey.
(b) When DPD is applied to (a). The measured ACLR is printed in black.
(c) Spectrum of estimation signal. Spectrum of validation signal was similar.

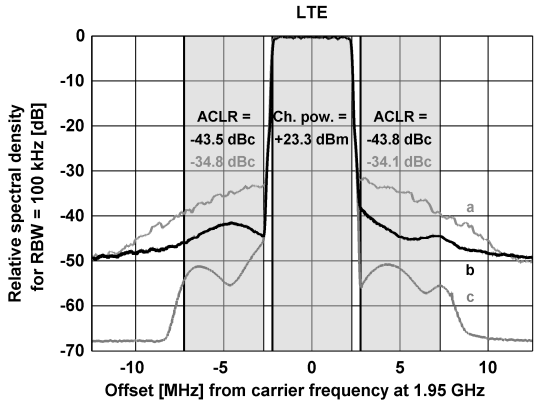

Fig. 16. Measured LTE spectrum at 1.95 GHz.
(a) Measured LTE spectrum without DPD. The measured ACLR is printed in grey.
(b) When DPD is applied to (a). The measured ACLR is printed in black.
(c) Spectrum of estimation signal. Spectrum of validation signal was similar.

standards. In measurements at 1.95 GHz, the DPD proved to be successful and improved the WCDMA ACLR at 5 MHz and 10 MHz offsets by 10.8 dB and 7.5 dB, respectively. The LTE ACLR at 5 MHz offset was improved by 9.4 dB. Thus, the predistortion method improves the measured ACLR to have at least 12.6 dB of margin to the requirements [51], [52]. The measured ACLR at 5 MHz is comparable to state-of-the-art WCDMA [53], [54] transceivers.

Assuming a PA with 35 dB of dynamic range (neglecting phase distortions), i.e. assuming g_1 = 0.509 and g_2 = 0.491, and a polynomial degree of $n = 5$, the computed achievable ACLR at 5 MHz and 10 MHz is ∼3 dB better compared to the measurements with the WCDMA signal. Similarly, the computed achievable ACLR at 5 MHz is ∼2 dB better compared to the measurements with the LTE signal.

The sampling rate was 92.16 MHz in the measurements, six times the original sampling frequency of the signal, and was chosen as high as possible while still being able to practically map the measured IQ data with the estimation signal. The impact of baseband filtering and limited bandwidth

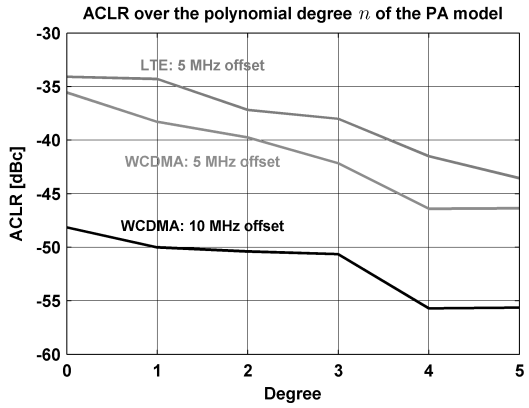

Fig. 17. Measured ACLR depending on the polynomial degree n of the PA model. Degree = 0 represents the performance without predistortion.

is investigated in [55] and [56], where it was concluded that to obtain an optimal signal/distortion ratio over the entire bandwidth, a compromise between the sampling frequency and the filter characteristics has to be made. In this paper, we have evaluated the required bandwidth/sampling rate based on measurements with two signal generators and one combiner (no PA). Increasing the sampling frequency from the original 15.36 MHz to 30.72 MHz and 61.44 MHz, the ACLR at 5 MHz for the WCDMA signal improves from -44 dBc to -50 dBc and -52 dBc, respectively. Similarly, the ACLR at 10 MHz offset improves from -48 dBc to -52 dBc and -56 dBc, respectively. The corresponding improvements for the LTE signal at 5 MHz are -34 dBc to -43 dBc and -46 dBc. Thus, for the specific tests performed here, the ACLR at 5 and 10 MHz can improve by 6-9 dB and 4-8 dB, respectively, when increasing the sampling rate up to four times the original sampling rate of 15.36 MHz. Further increasing the sampling frequency, up to 92.16 MHz, shows no significant change.

IX. Conclusions

This paper presents a model-based phase-only predistortion method suitable for outphasing RF PAs. The model estimation has here been reformulated from a nonconvex problem into a convex least-squares problem, and the predistorter can be calculated analytically. The predistortion method has been applied at the signal generation level in the baseband, and it has been used for WCDMA and LTE uplink signals applied to a fully integrated +30 dBm Class-D outphasing RF PA in 65nm CMOS, which is one of the first fully integrated +30 dBm outphasing PAs. In measurements at 1.95 GHz, the DPD proved to be successful and improved the WCDMA ACLR at 5 MHz and 10 MHz offsets by 10.8 dB and 7.5 dB, respectively. The LTE ACLR at 5 MHz offset was improved by 9.4 dB.

Acknowledgment

The authors would like to thank Dr. Peter Olanders, Ericsson Research, Kista, Sweden, for useful discussions.

REFERENCES

[1] P. Reynaert and M. Steyaert, "A 1.75-GHz Polar Modulated CMOS RF Power Amplifier for GSM-EDGE," *IEEE J. Solid-State Circuits*, vol. 40, no. 12, pp. 2598–2608, Dec. 2005.

[2] D. Cox, "Linear Amplification with Nonlinear Components," *IEEE Trans. Comm.*, vol. COM-23, pp. 1942–1945, Dec. 1974.

[3] H. Chireix, "High Power Outphasing Modulation," *IRE*, vol. 23, pp. 1370–1392, Nov. 1935.

[4] A. Pham and C. Sodini, "A 5.8GHz, 47% Efficiency, Linear Outphase Power Amplifier with Fully Integrated Power Combiner," in *IEEE Radio Freq. Integrated Circuits Symp. (RFIC)*, Jun. 2006.

[5] A. Birafane and A. Kouki, "Phase-Only Predistortion for LINC Amplifiers With Chireix-Outphasing Combiners," *IEEE Trans. Microw. Theory Tech.*, vol. 53, no. 6, pp. 2240–2250, Jun. 2005.

[6] H. Xu, Y. Palaskas, A. Ravi, M. Sajadieh, M. El-Tanani, and K. Soumyanath, "A Flip-Chip-Packaged 25.3dBm Class-D Outphasing Power Amplifier in 32nm CMOS for WLAN Application," *IEEE J. Solid-State Circuits*, vol. 46, no. 7, pp. 1596–1605, Jul. 2011.

[7] P. Godoy, D. Perreault, and J. Dawson, "Outphasing Energy Recovery Amplifier with Resistance Compression for Improved Efficiency," *IEEE Trans. Microw. Theory Tech.*, vol. 57, no. 12, pp. 2895–2906, Dec. 2009.

[8] I. Hakala, D. Choi, L. Gharavi, N. Kajakine, J. Koskela, and R. Kaunisto, "A 2.14-GHz Chireix Outphasing Transmitter," *IEEE Trans. Microw. Theory Tech.*, vol. 53, no. 6, pp. 2129–2138, Jun. 2005.

[9] S. Moloudi, K. Takanami, M. Youssef, M. Mikhemar, and A. Abidi, "An Outphasing Power Amplifier for Software-Defined Radio Transmitter," in *ISSCC Dig. Tech. Papers*, Feb. 2008, pp. 568–569.

[10] A. Birafane and A. Kouki, "On the Linearity and Efficiency of Outphasing Microwave Amplifiers," *IEEE Trans. Microw. Theory Tech.*, vol. 52, no. 7, pp. 1702–1708, Jun. 2004.

[11] W. Tai, H. Xu, A. Ravi, H. Lakdawala, O. Degani, L. Carley, and Y. Palaskas, "A +31.5dBm Outphasing Class-D Power Amplifier in 45nm CMOS with Back-Off Efficiency Enhancement by Dynamic Power Control," in *IEEE Europ. Solid-State Circuits Conf. (ESSCIRC)*, Sep. 2011, pp. 131–134.

[12] H. Xu, Y. Palaskas, A. Ravi, and K. Soumyanath, "A Highly Linear 25dBm Outphasing Power Amplifier in 32nm CMOS for WLAN Application," in *IEEE Europ. Solid-State Circuits Conf. (ESSCIRC)*, Sep. 2010, pp. 306–309.

[13] J. Fritzin, C. Svensson, and A. Alvandpour, "A Class-D Outphasing RF Amplifier with Harmonic Suppression in 90nm CMOS," in *IEEE Europ. Solid-State Circuits Conf. (ESSCIRC)*, Sep. 2010, pp. 310–313.

[14] ——, "A +32dBm 1.85GHz Class-D Outphasing RF PA in 130nm CMOS for WCDMA/LTE," in *IEEE Europ. Solid-State Circuits Conf. (ESSCIRC)*, Sep. 2011, pp. 127–130.

[15] ——, "A Wideband Fully Integrated +30dBm Class-D Outphasing RF PA in 65nm CMOS," in *IEEE International Symp. on Integrated Circuits (ISIC)*, Dec. 2011., pp. 25–28.

[16] J. Fritzin, Y. Jung, P. Landin, P. Händel, M. Enqvist, and A. Alvandpour, "Phase Predistortion of a Class-D Outphasing RF Amplifier in 90nm CMOS," *IEEE Trans. Circuits Syst.-II: Express Briefs*, vol. 58, no. 10, pp. 642–646, Oct. 2011.

[17] J. Yao and S. Long, "Power Amplifier Selection for LINC Application," *IEEE Trans. Circuits Syst.-II: Express Briefs*, vol. 53, no. 8, pp. 763–766, Aug. 2006.

[18] S. Hamedi-Hagh and A. Salama, "CMOS Wireless Phase-Shifted Transmitter," *IEEE J. Solid-State Circuits*, vol. 39, no. 8, pp. 1241–1252, Aug. 2004.

[19] T.-P. Hung, D. Choi, L. Larson, and P. Asbeck, "CMOS Outphasing Class-D Amplifier With Chireix Combiner," *IEEE Microwave and Wireless Components Letters*, vol. 17, no. 8, pp. 619–621, Aug. 2007.

[20] S. Lee and S. Nam, "A CMOS Outphasing Power Amplifier With Integrated Single-Ended Chireix Combiner," *IEEE Trans. Circuits Syst.-II: Express Briefs*, vol. 57, no. 6, pp. 411–415, Jun. 2010.

[21] A. Birafane, M. El-Asmar, A. Kouki, M. Helaoui, and F. Ghannouchi, "Analyzing LINC Systems," *IEEE Microwave Magazine*, vol. 11, no. 5, pp. 59–71, Aug. 2010.

[22] L. Romano, L. Panseri, C. Samori, and A. Lacaita, "Matching Requirements in LINC Transmitters for OFDM Signals," *IEEE Trans. Circuits Syst. I, Reg. Papers*, vol. 53, no. 7, pp. 1572–1578, Jul. 2006.

[23] A. Zhu, P. Draxler, J. Yan, T. Brazil, D. Kimball, and P. Asbeck, "Open-Loop Digital Predistorter for RF Power Amplifiers Using Dynamic Deviation Reduction-Based Volterra Series," *IEEE Trans. Microw. Theory Tech.*, vol. 56, no. 7, pp. 1524–1534, Jul. 2008.

[24] A. Zhu, P. Draxler, C. Hsia, T. Brazil, D. Kimball, and P. Asbeck, "Digital Predistortion for Envelope-Tracking Power Amplifiers Using Decomposed Piecewise Volterra Series," *IEEE Trans. Microw. Theory Tech.*, vol. 56, no. 10, pp. 2237–2247, Oct. 2008.

[25] L. Guan and A. Zhu, "Low-Cost FPGA Implementation of Volterra Series-Based Digital Predistorter for RF Power Amplifiers," *IEEE Trans. Microw. Theory Tech.*, vol. 58, no. 4, pp. 866–872, Apr. 2010.

[26] L. Anttila, P. Händel, and M. Valkama, "Joint Mitigation of Power Amplifier and I/Q Modulator Impairments in Broadband Direct-Conversion Transmitters," *IEEE Trans. Microw. Theory Tech.*, vol. 58, no. 4, pp. 730–739, Apr. 2010.

[27] J. Mehta, V. Zoicas, O. Eliezer, R. Staszewski, S. Rezeq, M. Entezari, and P. Bolsara, "An Efficient Linearization Scheme for a Digital Polar EDGE Transmitter," *IEEE Trans. Circuits Syst.-II: Express Briefs*, vol. 57, no. 3, pp. 193–197, Mar. 2010.

[28] Y. Woo, J. Kim, J. Yi, S. Hing, I. Kim, J. Moon, and B. Kim, "Adaptive Digital Feedback Predistortion Technique for Linearizing Power Amplifiers," *IEEE Trans. Microw. Theory Tech.*, vol. 55, no. 5, pp. 932–940, May 2007.

[29] C. Presti, F. Carrara, A. Scuderi, P. Asbeck, and G. Palmisano, "A 25 dBm Digitally Modulated CMOS Power Amplifier for WCDMA/EDGE/OFDM with Adaptive Digital Predistortion and Efficient Power Control," *IEEE J. Solid-State Circuits*, vol. 44, no. 7, pp. 1883–1896, Jul. 2009.

[30] X. Zhang, L. Larson, P. Asbeck, and P. Nanawa, "Gain/Phase Imbalance-Minimization Techniques for LINC Transmitters," *IEEE Trans. Microw. Theory Tech.*, vol. 49, no. 12, pp. 2507–2516, Jun. 2001.

[31] S.-S. Myoung, I.-K. Kee, J.-G. Yook, K. Lim, and J. Laskar, "Mismatch Detection and Compensation Method for the LINC System Using a Closed-Form Expression," *IEEE Trans. Microw. Theory Tech.*, vol. 56, no. 12, pp. 3050–3057, Dec. 2008.

[32] A. Huttunen and R. Kaunisto, "A 20-W Chireix Outphasing Transmitter for WCDMA Base Stations," *IEEE Trans. Microw. Theory Tech.*, vol. 55, no. 12, pp. 2709–2718, Dec. 2007.

[33] T.-W. Chen, P.-Y. Tsai, J.-Y. Yu, , and C.-Y. Lee, "A Sub-mW All-Digital Signal Component Separator With Branch Mismatch Compensation for OFDM LINC Transmitters," *IEEE J. Solid-State Circuits*, vol. 46, no. 11, pp. 2514–2523, Nov. 2011.

[34] P. Landin, J. Fritzin, W. V. Moer, M. Isaksson, and A. Alvandpour, "Modeling and Digital Predistortion of Class-D Outphasing RF Power Amplifiers," *IEEE Trans. on Microw. Theory Tech.*, vol. 60, no. 6, pp. 1907–1915, June 2012.

[35] W. Rudin, *Principles of Mathematical Analysis*, 3rd ed. McGraw-Hill Book Co., 1976.

[36] L. Ljung, *System Identification, Theory for the user*, 2nd ed. Prentice Hall PTR, 1999.

[37] S. Boyd and L. Vandenberghe, *Convex Optimization*. Cambridge University Press, 2004.

[38] Å. Björck, *Numerical Methods for Least Squares Problems*. Siam, 1996.

[39] G. Montoro, P. Gilabert, E. Bertran, A. Cesari, and J. Garcia, "An LMS-Based Adaptive Predistorter for Cancelling Nonlinear Memory Effects in RF Power Amplifiers," in *Microwave Conference, 2007. APMC 2007. Asia-Pacific*, Dec. 2007.

[40] P. Gilabert, E. Bertran, G. Montoro, and J. Berenguer, "FPGA Implementation of an LMS-based Real-Time Adaptive Predistorter for Power Amplifiers," in *Circuits and Systems and TAISA Conference, 2009. NEWCAS-TAISA '09. Joint IEEE North-East Workshop on*, June-July 2009.

[41] J. Walling, H. Lakdawala, Y. Palaskas, A. Ravi, O. Degani, K. Soumyanath, and D. Allstot, "A Class-E PA With Pulse-Width and Pulse-Position Modulation in 65nm CMOS," *IEEE J. Solid-State Circuits*, vol. 44, no. 6, pp. 1668–1678, Jun. 2011.

[42] J. Fritzin, C. Svensson, and A. Alvandpour, "Design and Analysis of a Class-D Stage with Harmonic Suppression," *IEEE Trans. Circuits Syst.-I: Regular Papers*, vol. 59, no. 6, pp. 1178–1186, June 2012.

[43] Rohde & Schwarz, Application note, 1GP67: Phase Adjustment of Two MIMO Signal Sources with Option B90.

[44] L. Larcher, D. Sanzogni, R. Brama, A. Mazzanti, and F. Svelto, "Oxide Breakdown After RF Stress: Experimental Analysis and Effects on Power Amplifier Operation," in *IEEE Reliability Physics Symposium*, Mar. 2006, pp. 283–288.

[45] J. Stauth and S. Sanders, "A 2.4GHz, 20dBm Class-D PA with Single-Bit Digital Polar Modulation in 90nm CMOS," in *IEEE Custom Integrated Circuits Conf. (CICC)*, Sep. 2008, pp. 737–740.

[46] D. Chowdhury, L. Yu, E. Alon, and A. Niknejad, "A 2.4 GHz Mixed-Signal Polar Power Amplifier with Low-Power Integrated Filtering in

65nm CMOS," in *IEEE Custom Integrated Circuits Conf. (CICC)*, Sep. 2010.
[47] ——, "An Efficient Mixed-Signal 2.4-GHz Polar Power Amplifier in 65nm CMOS," *IEEE J. Solid-State Circuits*, vol. 46, no. 8, pp. 1796–1809, Aug. 2011.
[48] S.-M. Yoo, J. Walling, E. Woo, and D. Allstot, "A Switched-Capacitor Power Amplifier for EER/Polar transmitters," in *ISSCC Dig. Tech. Papers*, Feb. 2011, pp. 427–428.
[49] S.-M. Yoo, J. Walling, E. Woo, B. Jann, and D. Allstot, "A Switched-Capacitor RF Power Amplifier," *IEEE J. Solid-State Circuits*, vol. 46, no. 12, pp. 2977–2987, Dec. 2011.
[50] H. Xu, Y. Palaskas, A. Ravi, M. Sajadieh, M. Elmala, and K. Soumyanath, "A 28.1dBm class-D Outphasing Power Amplifier in 45nm LP Digital CMOS," in *VLSI Symp.*, Jun. 2009, pp. 206–207.
[51] 3GP TS 25.101 v10.2.0 (2011-06). 3rd Generation Partnership Project; Technical Specification Group Radio Access Network; User Equipment (UE) radio transmission and reception (FDD), Release 10.
[52] 3GPP TS 36.101 v10.3.0 (2011-06). 3rd Generation Partnership Project; Technical Specification Group Radio Access Network; Evolved Universal Terrestrial Radio Access (E-UTRA); User Equipment (UE) radio transmission and reception, Release 10.
[53] Q. Huang, J. Rogin, X. Chen, D. Tschopp, T. Burger, T. Christen, D. Papadopolous, I. Kouchev, C. Martelli, and T. Dellsperger, "A Tri-Band SAW-Less WCDMA/HSPA RF CMOS Transceiver, with On-Chip DC-DC Converter Connectable to Battery," in *ISSCC Dig. Tech. Papers*, Feb. 2010, pp. 60–61.
[54] M. Ingels, V. Giannini, J. Borremans, G. Mandal, B. Debaillie, P. van Wesemael, T. Sano, T. Yamamoto, D. Hauspie, J. van Driessche, and J. Craninckx, "A 5mm^2 40nm LP CMOS 0.1-to-3GHz Multistandard Transceiver," in *ISSCC Dig. Tech. Papers*, Feb. 2010, pp. 458–459.
[55] W. Gerhard and R. Knöchel, "Prediction of bandwidth requirements for a digitally based WCDMA phase modulated outphasing transmitter," in *The European Conference on Wireless Technology*, 2005, pp. 97–100.
[56] ——, "LINC Digital Component Separator for Single and Multicarrier W-CDMA Signals," *IEEE Trans. Microw. Theory Tech.*, vol. 53, no. 1, pp. 274–282, Jan. 2005.

Ylva Jung was born in Stockholm, Sweden, in 1984 and recieved her M.Sc. degree in Applied Physics and Electrical Engineering from Linköping University, Linköping, Sweden, in 2010. At present, she is working towards a Ph.D. degree at the at the Division of Automatic Control within the Department of Electrical Engineering, Linköping University. Her main research interest is system inversion of nonlinear dynamics with focus on power amplifier predistortion.

Jonas Fritzin (S07-M12) received his M.Sc. degree in electrical engineering from Chalmers University of Technology, Göteborg, Sweden, in 2004 and the Ph.D. degree from Linköping University, Linköping, Sweden, in 2011. Since 2012 he is working with research and development of analog/RF IC for future base stations at Ericsson AB, Stockholm, Sweden. His research interests include CMOS RF power amplifiers, transmitters, and predistortion.

Martin Enqvist (M08) was born in Lund, Sweden in 1976. He obtained the M.Sc. degree in Applied Physics and Electrical Engineering in 2000 and the Ph.D. degree in Automatic Control in 2005, both from Linköping University, Sweden. During 2006, he worked as a postdoctoral researcher at Vrije Universiteit Brussel in Belgium and he is currently an associate professor at the Department of Electrical Engineering at Linköping University. His main research interest is in the field of nonlinear system identification.

Atila Alvandpour (M99-SM04) received the M.S. and Ph.D. degrees from Linköping University, Sweden, in 1995 and 1999, respectively. From 1999 to 2003, he was a senior research scientist with Circuit Research Lab, Intel Corporation. In 2003, he joined the department of Electrical Engineering, Linköping University, as a Professor of VLSI design. Since 2004, he is the head of Electronic Devices division. He is also the coordinator of Linköping Center for Electronics and Embedded Systems (LINCE). His research interests include various issues in design of integrated circuits and systems in advanced nanoscale technologies, with a special focus on efficient analog-to-digital data converters, wireless transceiver front-ends, sensor interface electronics, high-speed signaling, on-chip clock generators and synthesizers, low-power/high-performance digital circuits and memories, and chip design techniques. He has published about 100 papers in international journals and conferences, and holds 24 U.S. patents. Prof. Alvandpour is a senior member of IEEE, and has served on many technical program committees of IEEE and other international conferences, including the IEEE Solid-State Circuits Conference, ISSCC, and European Solid-State Circuits Conference, ESSCIRC. He has also served as guest editor for IEEE Journal of Solid-State Circuits.